1991

The Seasonal Circulation of the Upper Ocean in the Bay of Bengal

James T. Potemra
Florida State University

Mark E. Luther
University of South Florida, mluther@usf.edu

JOURNAL OF GEOPHYSICAL RESEARCH, VOL. 96, NO. C7, PAGES 12,667–12,683, JULY 15, 1991

The Seasonal Circulation of the Upper Ocean in the Bay of Bengal

JAMES T. POTEMRA,[1] MARK E. LUTHER,[2] AND JAMES J. O'BRIEN

Mesoscale Air-Sea Interaction Group, Florida State University, Tallahassee

Analysis of the results of a multilayer, adiabatic, numerical model of the upper Indian Ocean, driven by climatological monthly mean winds, shows that the simulated currents in the northeastern Indian Ocean are in general agreement with available observations and interpretations. The main features of the ocean currents include large anticyclonic flow in the Bay of Bengal surface waters during the northern hemisphere winter. This gyre decays into eddies in spring and then transitions into a weaker, cyclonic gyre by late summer. The western recirculation region of this flow is an intensified western boundary current which changes direction twice during the year. In the Andaman Sea, east of the Bay of Bengal, the oceanic flow changes direction twice during the year; it is cyclonic during the spring and early summer and anticyclonic the rest of the year. Flow in the equatorial region shows the North Equatorial Current (NEC) flowing west during winter. Further south is the eastward flowing Equatorial Counter Current (ECC) and the westward flowing South Equatorial Current. In summer, the NEC switches direction, joins the ECC, and forms the Indian Monsoon Current. Investigation of the second layer of the model (the upper 450 m of the ocean) shows that flow during much of the year is baroclinic (strong vertical shear). Model layer thickness reveals coastal Kelvin waves propagating along the coast, traveling the entire perimeter of the Andaman Sea and the Bay of Bengal. This wave excites westward propagating Rossby waves into the interior of the bay. Time series analysis of transport calculations yield significant peaks in the 20- to 30-day range and 50- to 60-day range which are not likely directly forced by the applied wind stress.

1. INTRODUCTION

The Indian Ocean is a particularly interesting, dynamically rich area because of the changing wind patterns associated with the Indian Monsoon. In spite of this, it is a relatively poorly studied area. In addition, data coverage for the area is sparse. While some data sets do exist, they are predominantly on large space and time scales. Recent efforts, such as the monsoon experiment (MONEX) of the Global Atmospheric Research Program (GARP), the First GARP Global Experiment (FGGE), and the Indian Ocean Experiment (INDEX), have substantially improved the availability of measured data in this region.

Individual studies have also contributed in recent years to the understanding of the dynamics in the Indian Ocean. An early effort by *Wyrtki* [1961] synthesized the available data sets (at the time) of the properties of the Southeast Asian waters. More recently, *Legeckis* [1987] demonstrated the appearance of a western boundary current in the Bay of Bengal using sea surface temperature data obtained from the advanced very high resolution radiometer (AVHRR) carried on board the NOAA 9 satellite. Data coverage from this satellite encompasses the entire region of the Bay of Bengal [*McClain et al.*, 1985]. *Rao et al.* [1989] have generated mean monthly mixed layer depth, sea surface temperature, and surface current climatologies for the tropical Indian Ocean. *Molinari et al.* [1960] analyzed three different sets of satellite-tracked drifting buoys and compiled a monthly climatology of surface currents in the tropical Indian Ocean.

Finally, oceanic data for the Indian Ocean is compiled in a few excellent atlases [see *Düing*, 1970; *Wyrtki*, 1971; *Hastenrath and Lamb*, 1979; *Cutler and Swallow*, 1984]. Although these sources contribute significantly to the understanding of dynamics in the tropical Indian Ocean, data on smaller scales, particularly in the Bay of Bengal, are somewhat limited.

The focus of this study therefore is to use a realistic, wind-driven model to simulate ocean currents in the region of the Bay of Bengal, from 75°E to 111°E and from 7°S to 23°N. Similar studies have been done for other areas of the Indian Ocean [*Jensen*, 1990] and using different models [*Woodberry et al.*, 1989]. A review of modeling efforts in the Indian Ocean is given by *Luther* [1987]. The results of the model are compared with measured data in an attempt to understand the dynamics of the area. The model used for this study, developed at the Florida State University [*Jensen*, 1990], is a reduced gravity, three and one-half layer model.

Since the model has multiple layers, the subsurface currents can be studied as well as the surface. The lowest layer is at rest, however, and only the results from the first (surface) and second (subsurface) layers will be examined here.

Figure 1 shows the typical large-scale circulation pattern associated with the winter and summer monsoons as compiled in *Monatskarten für den Indischen Ozean* (*Deutsches Hydrographisches Institut* [1960], as depicted by *Düing* [1970]). The general surface circulation of the region in northern winter includes large anticyclonic flow in the Bay of Bengal, a westward flowing North Equatorial Current (NEC), and eastward flowing Equatorial Counter Current (ECC) and a westward flowing South Equatorial Current (SEC). The northern summer pattern is characterized by counterrotating eddies in the Bay of Bengal [*Düing*, 1970], an eastward flowing Indian Monsoon Current (IMC) and a westward flowing SEC.

The model reproduces these flows, in general agreement with the atlases previously discussed. In this presentation the model is first described. Next, a description of the

[1]Now at STX, NASA Goddard Space Flight Center, Greenbelt, Maryland.

[2]Now at Department of Marine Science, University of South Florida, St. Petersburg,.

Paper number 91JC01045.
0148-0227/91/91JC-01045$05.00

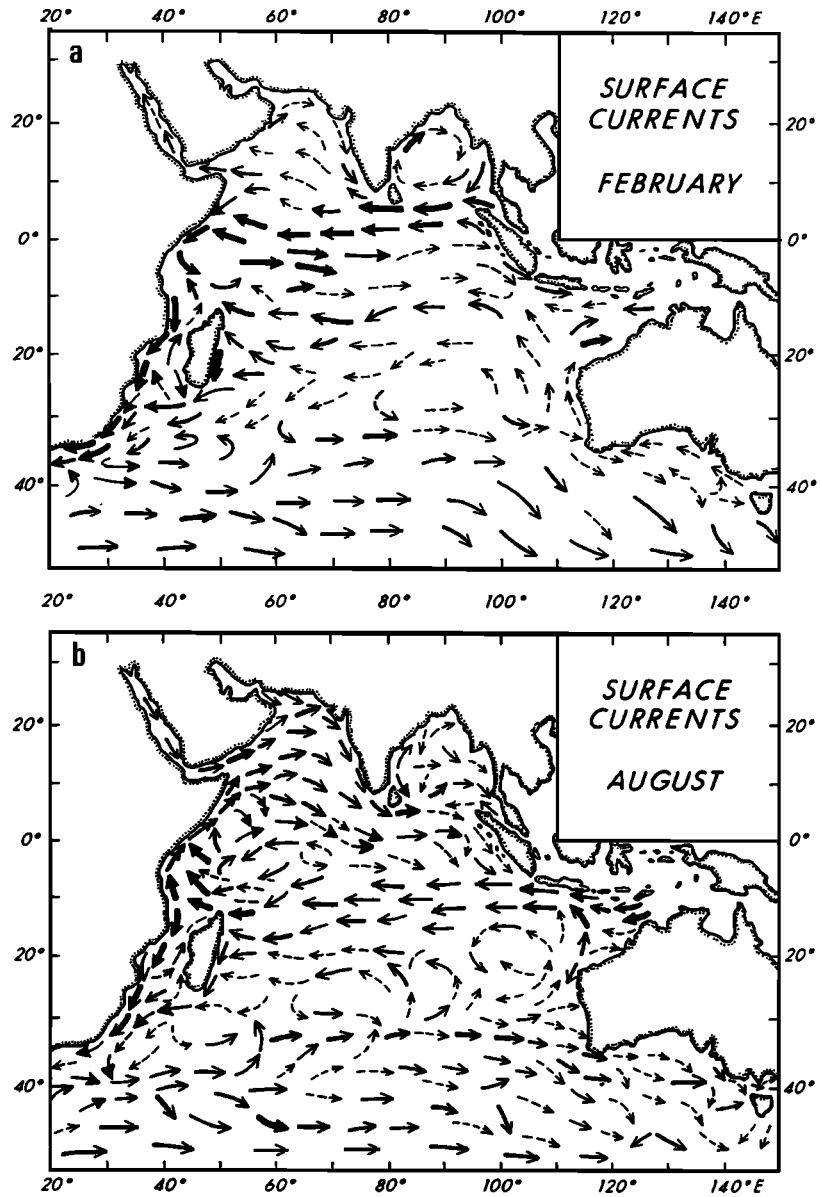

Fig. 1. Large-scale circulation as observed during (*a*) the winter (northeast) monsoon, and (*b*) the summer (southwest) monsoon. (*Deutsches Hydrographisches Institut* [1960], courtesy of W. Düing).

climatology of the winds that force the model is given. Finally, the results of the model are presented, first in terms of general circulation patterns and later in terms of oscillations of certain features.

2. Model

Isopycnic layered models have proven to be useful in the study of ocean dynamics. The work of *Luther and O'Brien* [1985] and *Luther et al.* [1985] demonstrates how a reduced gravity model can correctly simulate the currents of the western Indian Ocean. Further, *Woodberry et al.* [1989] show this model to be equally capable of reproducing the complex current system of the southern Indian Ocean. The success of these efforts gives rise to the numerical model used for this investigation of currents in the Bay of Bengal.

The model employed for this study was developed at the Florida State University by *Jensen* [1990] and is based on the work of Luther and O'Brien. This model, however, is composed of four isopycnal layers. The advantage of a multilayered model is the ability of studying both surface and subsurface currents. In addition, multiple layers provide greater accuracy in representing low vertical modes.

The layers of this model are assumed to have positive thickness everywhere at all times. In other words, the layers can not merge or surface, and the bottom topography is always in the lowest layer. The vertical modes for the Indian Ocean, given by *Gent et al.* [1983], are used to select the initial layer thicknesses and densities. The four densities are chosen to be 1023.9, 1026.2, 1027.3, and 1027.9 kg m^{-3}. The initial thicknesses of the layers are taken as 200 m for the top layer, 250 m for the second layer, and 400 m for the third.

For this model, horizontal eddy viscosity is based on the velocity field so that a thin layer with large velocities would experience more friction than a thick layer with equivalent transport [*Jensen*, 1990]. The magnitude of the horizontal

friction coefficient is taken to be 750 $m^2\ s^{-1}$ [*Woodberry et al.*, 1989].

Wind forcing at the surface is the only vertical stress that is applied, and it acts as a body force on the upper layer. Forcing due to the gradient in atmospheric pressure is ignored, since when taken in comparison to the wind stress, it is negligible for mesoscale motion. The barotropic modes, which give rise to gravity waves of large phase speed, are removed with the assumption of zero pressure gradient in the lower layer (the reduced gravity approximation).

Following the procedure of *Jensen* [1990], the model equations become, in spherical coordinates,

$$\frac{\partial U_j}{\partial t} + \frac{1}{a\cos\theta}\frac{\partial}{\partial\phi}\left(\frac{U_j^2}{H_j}\right) + \frac{1}{a}\frac{\partial}{\partial\theta}\left(\frac{U_jV_j}{H_j}\right) - \frac{2U_jV_j}{aH_j\cot\theta}$$

$$-fV_j = \frac{-H_j}{\rho_j a\cos\theta}\left[\frac{\partial p_a}{\partial\phi} + \rho_j g\frac{\partial\eta}{\partial\phi} - g\sum_{i=1}^{j-1}(\rho_j-\rho_i)\frac{\partial H_i}{\partial\phi}\right] + \left(\frac{\tau_j^{\phi,t}}{\rho_j} - \frac{\tau_j^{\phi,b}}{\rho_j}\right) + F^{\phi} \quad (1)$$

$$\frac{\partial V_j}{\partial t} + \frac{1}{a\cos\theta}\frac{\partial}{\partial\phi}\left(\frac{U_jV_j}{H_j}\right) + \frac{1}{a}\frac{\partial}{\partial\theta}\left(\frac{V_j^2}{H_j}\right) + \frac{U_j^2 - V_j^2}{aH_j\cot\theta}$$

$$+fU_j = \frac{-H_j}{\rho_j a}\left[\frac{\partial p_a}{\partial\theta} + \rho_j g\frac{\partial\eta}{\partial\theta} - g\sum_{i=1}^{j-1}(\rho_j-\rho_i)\frac{\partial H_i}{\partial\theta}\right] + \left(\frac{\tau_j^{\theta,t}}{\rho_j} - \frac{\tau_j^{\theta,b}}{\rho_j}\right) + F^{\theta} \quad (2)$$

where

U_j, V_j zonal and meridional components of vertically integrated volume components for layer j;
H_h thickness of layer j;
ρ_j density layer of j;
P_a atmospheric pressure;
a radius of the Earth;
ϕ longitude;
θ latitude;
f Coriolis parameter;
g gravitational acceleration;
η surface displacement;
τ tangential stress due to vertical friction.

F^{ϕ} is the horizontal friction for U transport, given by

$$A\left\{H_j\nabla^2\left(\frac{U_j}{H_j}\right) - \frac{1}{a^2\cos^2\theta}\left[U_j(1-2\cos^2\theta) + 2\sin\theta H_j\frac{\partial}{\partial\phi}\left(\frac{V_j}{H_j}\right)\right]\right\} \quad (3)$$

and F^{θ} is the horizontal friction for V transport, given by

$$A\left\{H_j\nabla^2\left(\frac{V_j}{H_j} - \frac{1}{a^2\cos^2\theta}\left[V_j(1-2\cos^2\theta) + 2\sin\theta H_j\frac{\partial}{\partial\phi}\left(\frac{U_j}{H_j}\right)\right]\right\}\right. \quad (4)$$

The continuity equation is

$$\frac{\partial H_j}{\partial t} + \frac{1}{a\cos\theta}\left[\frac{\partial U_j}{\partial\phi} + \frac{\partial}{\partial\theta}(V_j\cos\theta)\right] = w_e \quad (5)$$

where w_e is the turbulent entrainment velocity between first and second layers.

This entrainment term is included to prevent the interface between the top two layers from surfacing; that is, the upper layer thickness cannot go to zero. This term is positive in the case when the upper layer thickness becomes less than a prescribed value H_{min} and negative for the same case in the second layer and is given by

$$w_e = \frac{(H_1 - H_{min})^2}{\tau_e H_{min}} \qquad H_1 \le H_{min}$$
$$w_e = 0 \qquad H_1 > H_{min} \quad (6)$$

For the bottom two layers this term is set to zero. The effect of this entrainment on the upper layer momentum balance is neglected. Incorporating this entrainment velocity only in the continuity equation represents turbulent entrainment where entrained water into the upper layer has zero velocity and is warmed instantaneously to the upper layer density. For this particular study, however, this adjustment is rarely active. The value for H_{min} is taken to be 60 m and the time constant τ_e is 1.2 hours.

The boundary conditions for this set of equations are given in two parts. First, for closed boundaries, i.e., land, the no-slip condition is incorporated. At coastal points, therefore, both components of the transport are set to zero. Next, for open boundaries, a Sommerfield radiation condition is applied. The solution at the boundary is first separated into its vertical modes, and the radiation condition is applied to each mode separately. The resulting current components for the boundary are computed as the sum of these vertical modes.

The only forcing is the applied wind stress. The wind forcing is based on wind stress values taken from a climatological monthly mean data set prepared by *Hellerman and Rosenstein* [1983]. A pseudostress is formed by dividing these data values by the product of an average drag coefficient and an air density. For this study a constant drag coefficient of 0.0015 and an air density of 1.2 kg m^{-3} are applied. A bicubic spline is then used to interpolate the data from their 2° resolution down to the model resolution.

The domain of the model is from 25.1°S to 26.1°N and from 34.8°E to 119.6°E. It should be noted that the model domain is much larger than the domain of interest for this study. Results are investigated only in a small section of the total model domain. The open boundaries for the model are along the 25°S parallel and along the 119°E meridian between Australia and Indonesia. Figure 2 shows the domain of the entire model, with a border outlining the region of interest for this study.

The land values are given by the 200-m isobath. It is for this reason that shallow areas, which pose a significant impedance to flow, such as the channel between India and Sri Lanka, appear as land. Additionally, the two island chains, Nicobar and Andaman, appear as solid stretches of land.

With these boundary conditions established, the equations are discretized, using a resolution of one tenth of a degree in both horizontal directions. This was done, for the spatial derivatives, using the Arakawa C grid, which is a mass- and

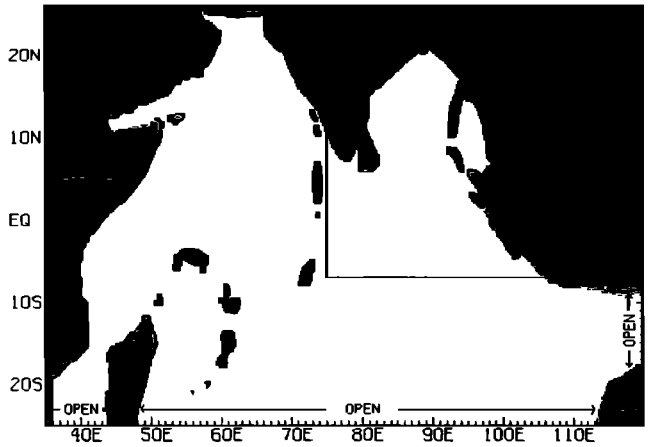

Fig. 2. Model domain. The 200-m isobath is used for land boundaries, and the open boundaries are labeled. The border in the northern part of the domain indicates the particular region investigated in this study.

energy-conserving scheme. The time integration was performed using an explicit leapfrog scheme with a forward Euler scheme applied every 99 time steps to remove the computational mode inherent to the leapfrog method. The Laplacian friction term is computed with a Dufort-Frankel implicit scheme [*O'Brien*, 1986] for computational convenience.

The model is spun up from rest, with a time step of 20 min, by repeatedly applying the annual wind stress cycle. After 10 years a quasi-periodic solution is obtained. The computer results are retained as fields of currents and layer thickness every 6 days.

3. Winds

Monsoon regions are considered to be those that experience the seasonal reversal in winds during the year. The Indian Ocean, characterized by large season to season variations due to the Asian monsoons, is one such region. In the Bay of Bengal area the winds are southwesterly during the northern summer months and switch to northeasterly during the months of the northern winter. The primary driving force for this oscillation in wind patterns is the differential heating between land and water [*Fein and Stephens*, 1987].

The wind patterns associated with the monsoon climate are compiled in the form of wind stress into a data set by *Hellerman and Rosenstein* [1983]. The model was forced by this climatological wind data set. This set was obtained by processing surface observations for approximately 100 years (1870–1976) and calculating monthly norms and standard deviations of the eastward and northward components of wind stress at standard anemometer height (10 m).

Figures 3*a* and 3*b* represent the wind conditions of January and July (the contours shown are the pseudostress values used to force the model). These are representative of the extreme conditions of the winter and summer monsoons, respectively. The months of April and October, shown in Figures 3*c* and 3*d*, demonstrate the transition period between the monsoon seasons. A more complete picture of the atmospheric conditions of the Indian Ocean can be found in the atlas by *Hastenrath and Lamb* [1979].

During the northern hemisphere winter monsoon months of November to February, the winds flow from the high pressure area over the Asian continent into the Bay of Bengal in a southwestward direction. These winds reach a maximum of about 6 m s^{-1} off the east coast of India during the month of December. In the beginning stages of the winter monsoon (November) the winds in the bay itself have a strong westward component down to approximately 7°N. Below 7°N, down to approximately 5°S, the winds are very zonal toward the east. During winter, therefore, 7°N represents a line of cyclonic wind shear. This wind pattern moves south of the equator as the season progresses.

This pattern is manifest as a region of large positive wind stress curl in early winter over the Bay of Bengal, down to about 5°N. This region of positive wind stress curl moves south as a band between 10°N and the equator, bounded to the north and south by regions of negative wind stress curl, during the northern spring months.

During March and April the winter monsoon begins the transition to the summer monsoon. Anticyclonic winds develop over the bay and, in conjunction with the weak maximum in the pressure field, bring flow with a southerly component to the western and northern shores of the bay. During March, flow from about 10°N down to 5°N is mainly toward the west, while from the equator to about 10°S it is toward the east. This pattern breaks down with the full arrival of the summer monsoon in July. By May the winds are predominantly southwesterly, originating in the southern hemisphere and sweeping through the Bay of Bengal. At the peak of the summer monsoon in July, the maximum wind speeds are found over the center of the bay and are of the order of 10 m s^{-1}.

The summer wind stress curl is somewhat different than that seen in winter. The band of positive wind stress curl is much more narrow, extending from about 5°N to 15°N. In addition the patch of positive curl runs along the coast to the extreme north of the bay rather than running in a zonal direction. The maximum values appear off the coast of Sri Lanka.

4. Regional Circulation

The large-scale circulation in the northern Indian Ocean can be described in three parts. First, there is a large gyre system which develops in the Bay of Bengal, the recirculation portion of which is a western boundary current along the east coast of India [*Legeckis*, 1987]. The model simulates only wind-driven flow, but several factors could determine the circulation in this region. It has been suggested that the river systems of India contribute in a small way to the circulation in the Bay of Bengal [*Somayajulu et al.*, 1987]. One large system is the Ganges, which empties into the northern end of the bay. In addition, the severe weather associated with the monsoon affects circulation in the form of tide surges and fresh water input [*Johns et al.*, 1985].

Another component of the circulation in the northern Indian Ocean is the flow into and around the Andaman Sea, bounded by Malaysia in the east and the Nicobar and Andaman Island chains in the west. It could be expected that discrepancies between the model and measured results would be greatest in this region due to the geometry of the model. The model cannot produce flow through the Malacca Strait, since it is less deep than the 200-m depth contour that the model uses as land (closed boundary). Data records indicate, however, that flow does travel from the South

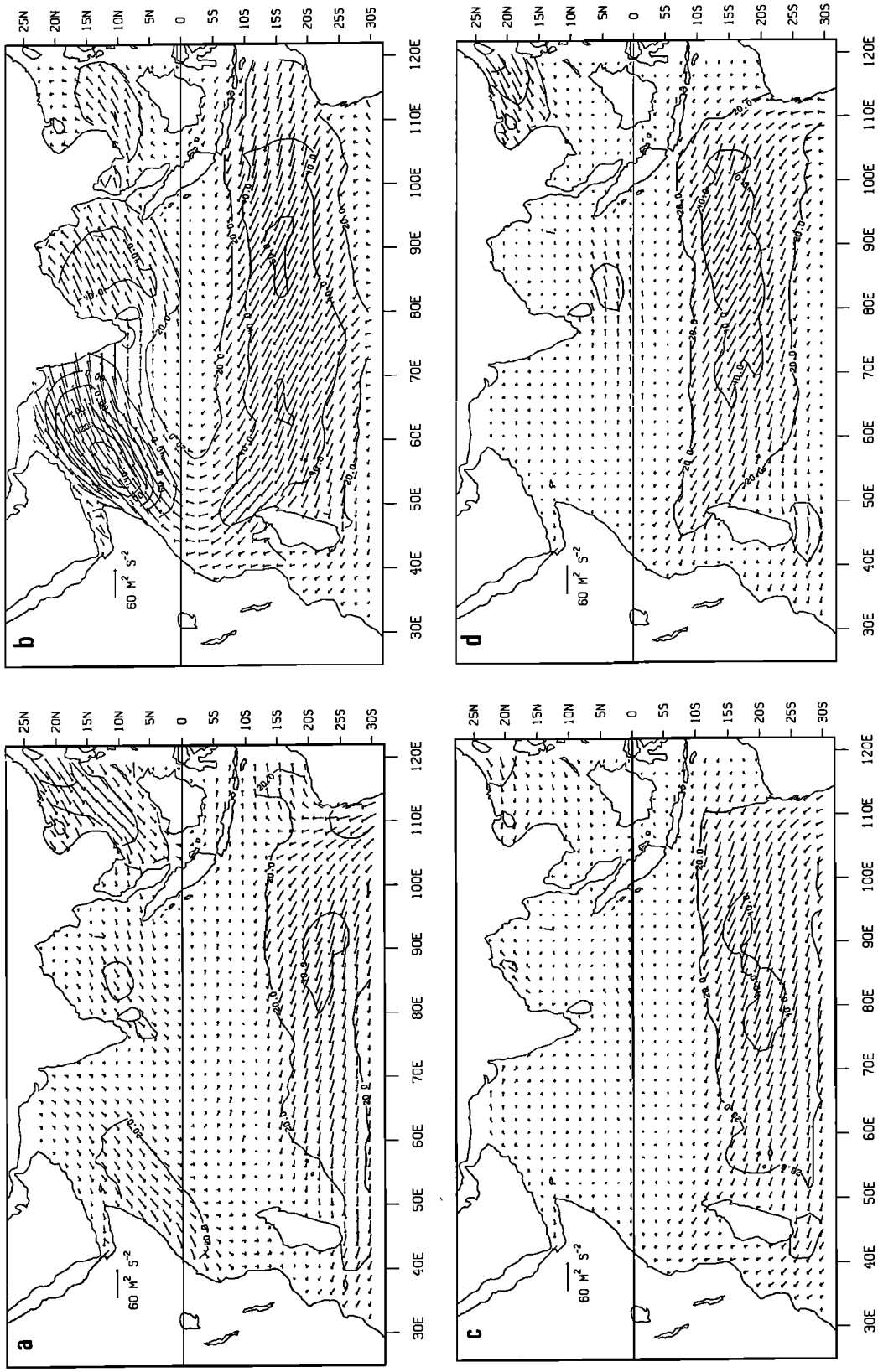

Fig. 3. Monthly mean wind fields for monsoon and transition periods. The vectors give direction for the wind field, while the contours give magnitude of the pseudostress. The contour interval is 20 $m^2 s^{-2}$. (*a*) Monthly mean wind field for January (winter monsoon). The winds come from the continent in a southwestward direction. They begin to weaken at the equator and turn eastward. South of the equator the atmospheric flow is predominantly to the east. The maximum wind velocities are found along 6°N. The minimum is centered about the equator. (*b*) Monthly mean wind field for July (summer monsoon). Winds in the Bay of Bengal are strictly toward the northeast, while south of the equator they are more northward in direction. The maximum for this time of year occurs in the center of the bay, and the minimum has moved to just south of the equator. (*c*) Monthly mean wind field for April (transition from the winter monsoon to the summer. An anticyclone has developed over the bay, fed by eastward flowing winds along the equator. The greatest wind speeds are found along the Indian mainland. (*d*) Monthly mean wind field for October (transition from the summer monsoon to the winter). Flow is eastward along the equator, turning northward at land. The velocities are somewhat weaker, with the maximum occurring just north of the equator.

China Sea into the Andaman Sea through this strait [*Cutler and Swallow*, 1984]. Similarly, the two island chains are treated by the model as single areas of land, allowing flow only between the two (through the Ten Degree Channel) and between Sumatra and Greater Nicobar Island (through the Great Channel). The model, therefore, treats the Andaman Basin as more of an enclosed area than actually exists.

The final components of the flow field in this region are the equatorial currents. These currents are the northern and southern extremes of gyres centered near the equator [*Molinari et al.*, 1990]. The northernmost current is the North Equatorial Current, which flows toward the west during northern winter, between 8°N and the equator [*Piccard and Emery*, 1982]. Further south, from the equator to 8°S, is the eastward flowing Equatorial Counter Current. During the summer monsoon, the NEC reverses direction, joins the ECC, and forms the Indian Monsoon Current [*Molinari et al.*, 1990]. In addition, an equatorial jet, explained by *O'Brien and Hurlburt* [1974], is formed during the monsoon transition periods (spring and fall) [*Wyrtki*, 1973]. This rapid, eastward flowing current is centered about the equator. Further south is the South Equatorial Current. The SEC flows from east to west all year, from about 15°S up to the ECC. While it does not change direction during the year, it does intensify in the northern summer months (May to September).

In addition to these surface currents, there is also a subsurface current, the Equatorial Undercurrent [*Cane*, 1980]. The EUC is found east of 60°E during the northern winter. It is weaker than its counterparts in the Pacific and Atlantic oceans, and during the northern summer, when equatorial flow is to the east, it is not evident [*Piccard and Emery*, 1982].

In this section these features are examined using the results of the multilayered, wind driven model. Whenever possible, comparisons with observed data are made. It should be noted, however, that the choice of an initial upper layer thickness affects the model-derived current speeds. For this investigation the initial upper layer thickness (based on *Gent et al.* [1983]) was taken as 200 m. Observations show a shallower mixed layer depth in this region [*Rao et al.*, 1989] which would explain why the in situ data of *Molinari et al.* [1990] shows a higher current speed than those given by the model. The large-scale features previously mentioned are, in fact, well represented by the model. Plate 1 shows the results of the model at six times during the year. The upper layer thickness, plotted using a color scale, gives an indication of the upper 200 m of the ocean. The current velocity is shown as vectors, with magnitude relative to the arrow length and direction given by the arrow orientation. Speeds less than 0.010 m s^{-1} are not displayed and speeds more than 0.100 m s^{-1} are truncated (to avoid making the figures too crowded).

Second interface topographies are shown in Plate 2. The field in this case represents the distance from the surface to the interface between the second and the third layers of the model. The velocity field is presented the same way as for the upper layer.

The features of both the surface and subsurface circulation can be readily identified from these figures. To get a more quantitative idea of the flow, transports were computed at certain cross sections using the model data. Figure 4 shows the locations where the calculations of mass transport were made. In the following sections, each part of the circulation previously outlined is described. The results of the transport computations are presented as they apply.

4.1. *The Bay of Bengal*

Examining first the results in the Bay of Bengal reveals a large anticyclonic gyre centered at 15°N, 86°E, fully established in February (see Plate 1*a*). This gyre is driven by the northeasterly wind of the winter monsoon. The gyre direction is consistent with the ship drift data of *Cutler and Swallow* [1984] and the observations of *Wyrtki* [1961] and *Tchernia* [1980]. The gyre intensifies on the western side, along the coast of India, as it travels northward. The appearance of this western boundary current is evident in satellite SST images of the area [*Legeckis*, 1987]. The buoy data of *Molinari et al.* [1990] reveal the gyre but do not show the western recirculation area (this may simply be due to the fact that a drifter buoy was not located in the relatively narrow recirculation region). Although the flow is usually baroclinic, at this time of the year it is somewhat barotropic, as evident by the similarity with the second layer results (Plate 2*a*). The center of the gyre appears at the thickest part of the two model layers. The thickness is 460 m at the center of the circulation (14°N, 82°E).

In March (Plate 1*b*) the anticyclonic gyre is still evident in the model results. The western boundary current is much more narrow, however. Along the coast, flow is northward but a few hundred kilometers offshore, and across the whole bay it is to the south. In addition, the upper layer thickness along the coast is less than in February, corresponding to a rise in the thermocline. This upwelling region extends along the coast all the way around the bay.

Flow in the lower layer (Plate 2*b*) shows the same narrowing of the gyre but also the formation of another. A cyclonic circulation has developed in the lower layer directly to the east of the first. It is centered at approximately 13°N, 87°E. The two gyres are joined at their southward branch, about 300 km from the coast of India.

Two months later, in May (Plate 1*c*), this upper layer appears unchanged, with upwelling along the coast somewhat less than earlier in the year. In the second layer the flow has reversed direction to a cyclonic orientation. The eastern gyre of the previous month has expanded westward and overridden the anticyclonic gyre that was there. This motion is being fed strongly by the eastward flow around the southern tip of Sri Lanka. The flow in May is more baroclinic, therefore, with flow in the upper layer opposing flow at deeper depths.

The flow in the next month, June, as displayed in Plates 1*d* and 2*d*, is even more baroclinic. The upper layer flow is northward along both coastlines. At about 17°N these two flows meet and turn south. A cyclonic circulation is thus established in the eastern portion of the bay with anticyclonic flow directly to the west. This resembles the subsurface flow of the preceding month. The upwelling region along the coast has propagated to the southern end of India, and it is followed by an area of downwelling; a region of deep upper layer thickness (200 m) is evident off the coast of Burma.

The cyclonic circulation flows around an area of shallow thickness; the interface depth is at a minimum of 440 m at the center of the gyre. By August, this area has moved north and hit the coast (Plate 2*e*). The anticyclonic flow in the lower

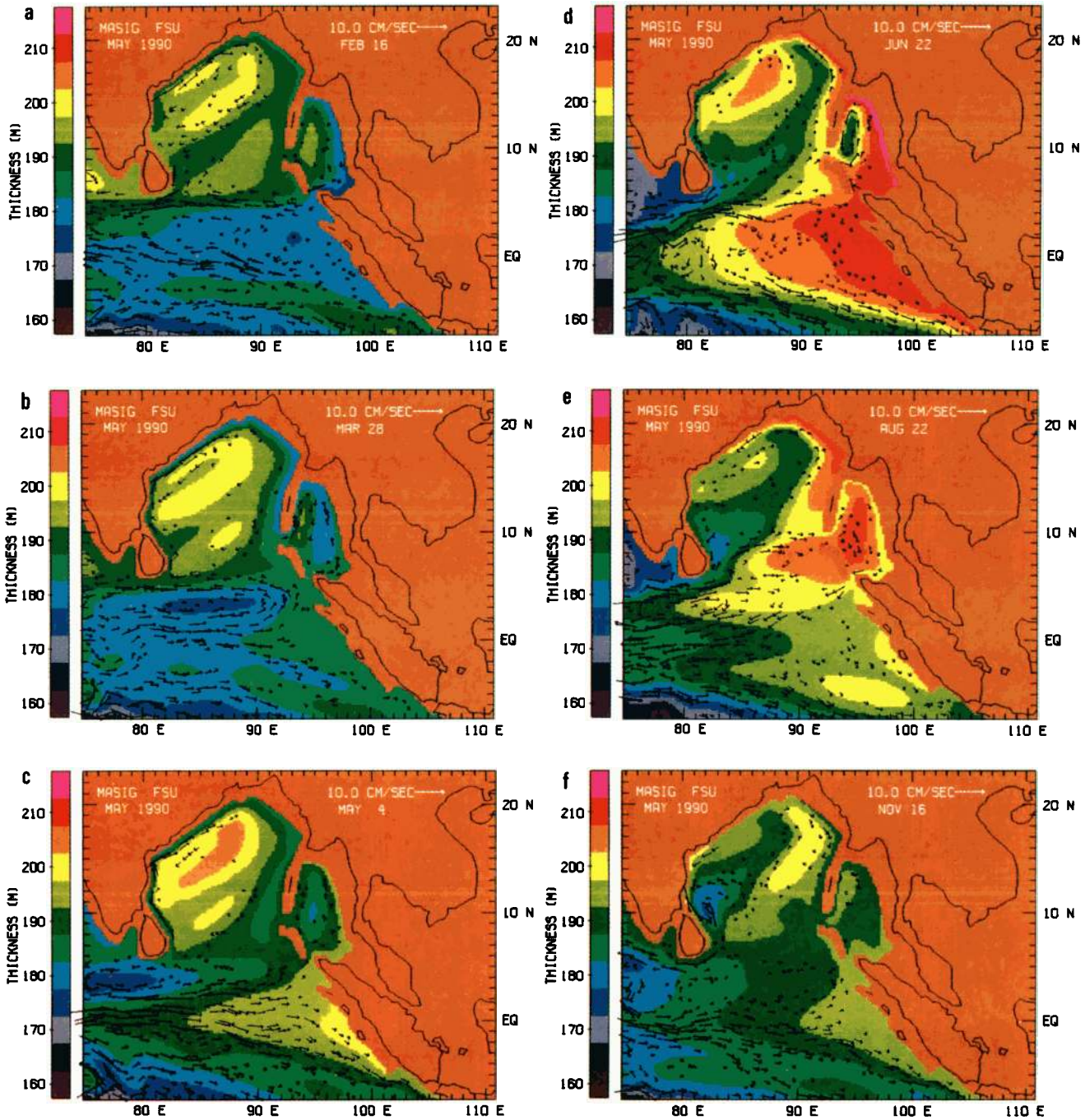

Plate 1. Model results for the surface layer, for (*a*) February, (*b*) March, (*c*) May, (*d*) June, (*e*) August, and (*f*) November. The thickness of the upper layer is represented by the color scale (in meters), and it reflects dynamic topography. The currents in the surface layer are given by the vectors. The major features of the circulation are the large circular flow in the Bay of Bengal, flow into and around the Andaman Sea, and the equatorial currents.

layer extends over most of the bay. The circulation in the upper layer during August is not quite the same as in the lower layer (Plate 1*e*). Flow is cyclonic throughout the entire bay. The region of downwelling has progressed westward around the top of the bay. Also, a region of upwelling has propagated northward around Sri Lanka. The upper layer thickness reaches a minimum of 175 m east of the island.

Toward the end of the year (Plates 1*f* and 2*f*), there is weak flow in both layers. The upper layer contains two rotating flows. One, anticyclonic around a region of downwelling, is in the northeastern corner of the bay. Flow along this large eddy is no more than a few centimeters per second, but this will develop into the large, bay-wide circulation of late winter (Plate 1*a*). In the southwest corner, a cyclonic circulation has developed around a region of upwelling centered at 10°N, 82°E.

Four stages of the flow in the Bay of Bengal emerge. The first is a large, anticyclonic gyre across the whole bay. This appears throughout the winter months (December until March). This is followed by two, counterrotating flows, anticyclonic on the western side and cyclonic on the eastern side, producing northward currents along both coasts and

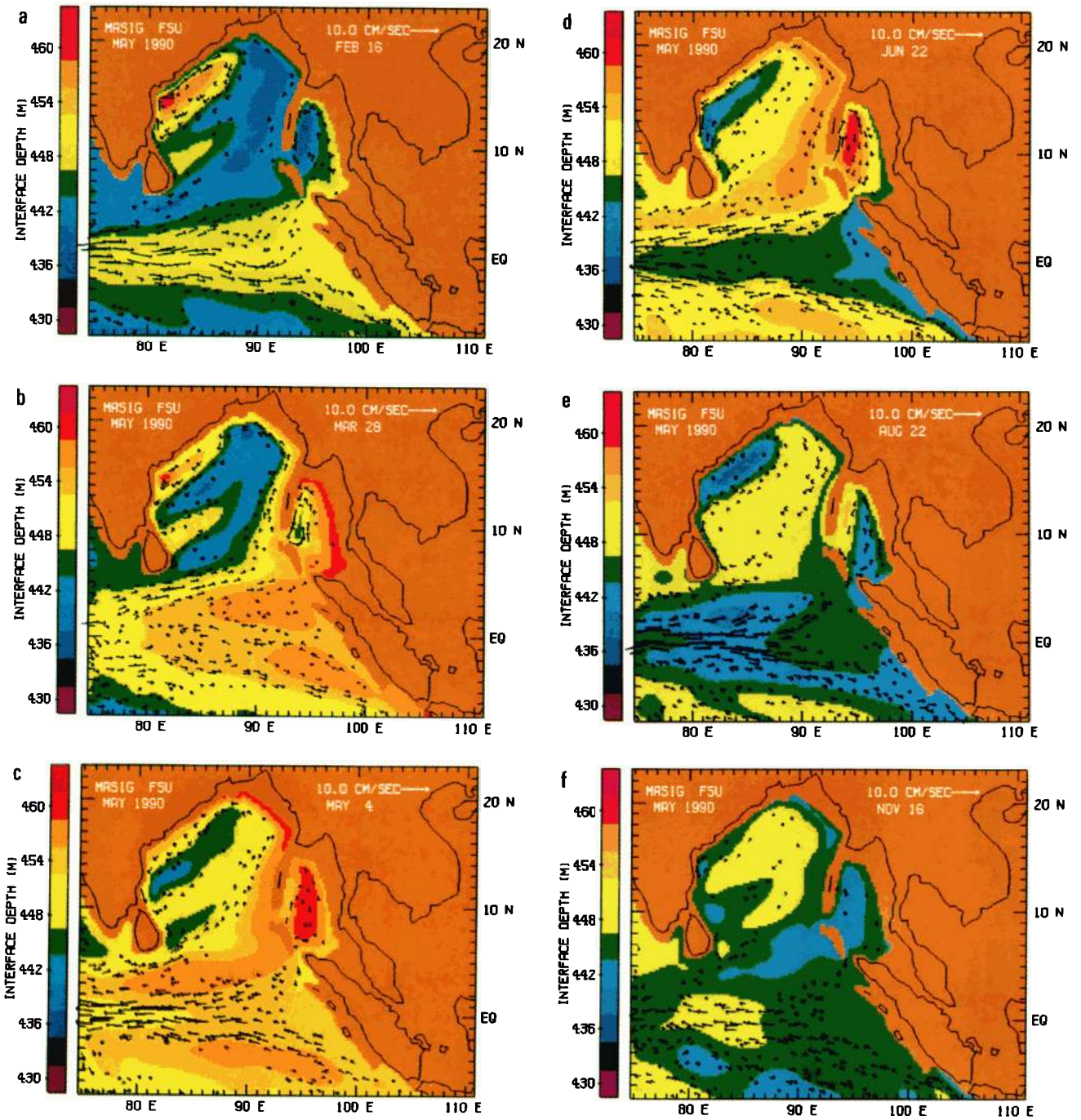

Plate 2. Model results for the second layer, for (*a*) February, (*b*) March, (*c*) May, (*d*) June, (*e*) August, and (*f*) November. The months are the same as in the case of the surface layer for comparison. The thickness represented by the color scale is the depth of the interface between the second and third layers.

southward flow down the middle. This persists until early summer (April–June) when the anticyclonic region dissipates and the cyclonic flow extends across the whole bay. The summer months of July and August are characterized by this large counterclockwise flow. In the fall, two rotating flows develop again, with southward currents along both coasts and northward flow in the center.

This pattern can be seen more quantitatively with the time series plots of mass transports of Figure 5. Transport is measured, using model data, at two transects on opposite sides of the bay (ST-1 and ST-2 of Figure 4). In this case, positive transport indicates northward flow, and negative transport reflects southward flow.

The four stages of the circulation are evident from these time series. The bay-wide, anticyclonic circulation of winter is apparent from the positive transport through ST-1 (northward flow) and the negative transport at ST-2 (southward flow). This occurs from December to March. Maximum transport along the western boundary current is 3.5 Sv during February in the upper layer. In the spring months of April, May and June two gyres are present, characterized by positive transport through both ST-1 and ST-2. Maximum

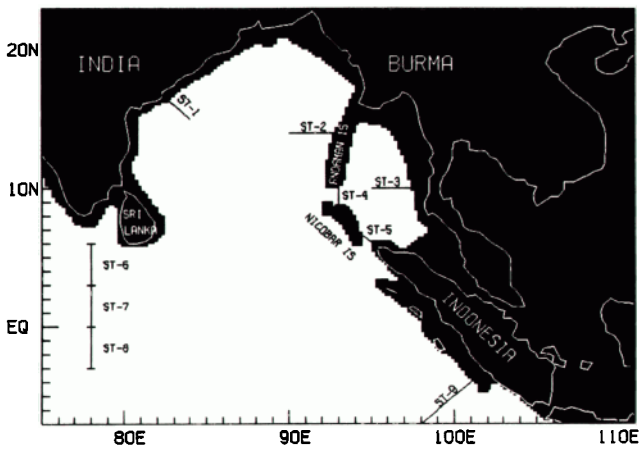

Fig. 4. Transect locations. Mass transport through nine stations is computed using model derived data. The first two stations (ST-1 and ST-2) are chosen to investigate flow in the Bay of Bengal. Three other stations (ST-3, ST-4, and ST-5) give an indication of flow in the Andaman Sea. The final four transects (ST-6, ST-7, ST-8, and ST-9) measure the equatorial flow.

transport at this time is 2 Sv in the western boundary. The other flow is very weak, with transport less than 1 Sv along the eastern coast. The eastern, weak cyclonic gyre expands westward, drowning out the anticyclonic flow, and encompasses the whole bay. In July and August transport is northward on the eastern side and negative on the western side. Maximum transport again is along the western boundary, and it reaches −1.20 Sv in late August. Finally, in the fall (September–November) the two-gyre system returns, this time with an anticyclonic circulation on the east side and cyclonic in the west. Transport reaches −2.0 Sv during early September in the western boundary current.

The transport calculated in the second layer reveals the baroclinicity of the circulation. The second layer anticyclonic gyre persists in December and January. Maximum transport occurs in the western boundary, reaching a value of 3.5 Sv in January. In February and March, while the upper layer still has southward flow along the eastern side of the bay, the lower layer begins to show northward (positive) transport on both sides. This develops into cyclonic flow in April and May. In June, July, and August, flow is southward along both coasts, similar to the two gyre system of the upper layer in fall. Finally in September, October, and November the flow is cyclonic throughout the whole bay.

4.2. *The Andaman Sea*

The flow in the Andaman Sea is less complicated than the flow in the Bay of Bengal. In March (Plate 1*b*) flow in the upper layer enters the sea south of the Nicobar Islands, circulates counterclockwise around the Andaman Basin and exits south of the Andaman Islands. This pattern continues

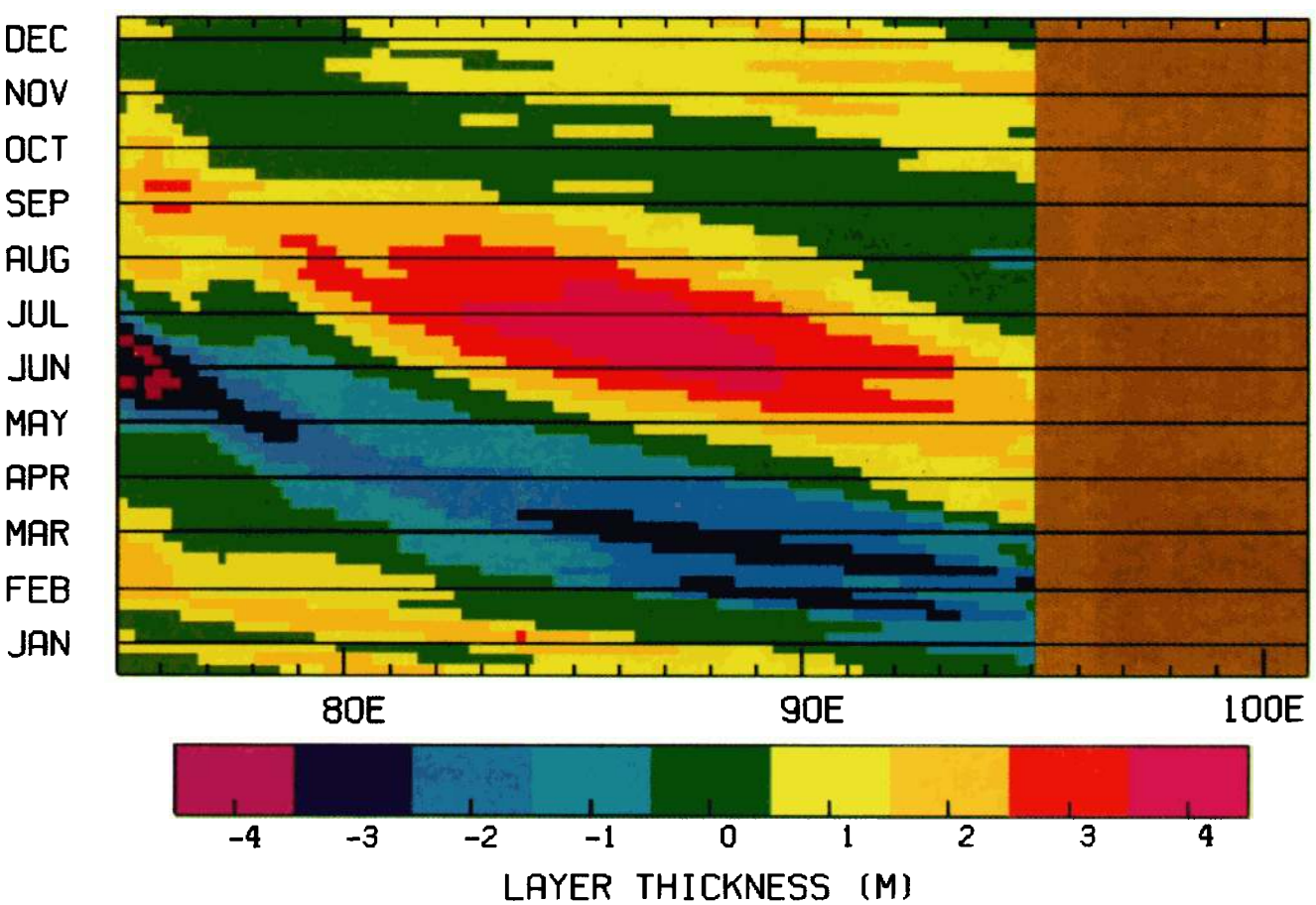

Plate 3. Antisymmetric component of the height field at 3°N. The sloping contour indicates a wave traveling west (phase velocity of 0.190 m s^{-1} to the west and period of 240 days). Because of the signal appearing in the antisymmetric plot and the phase velocity, these waves are interpreted as Rossby waves.

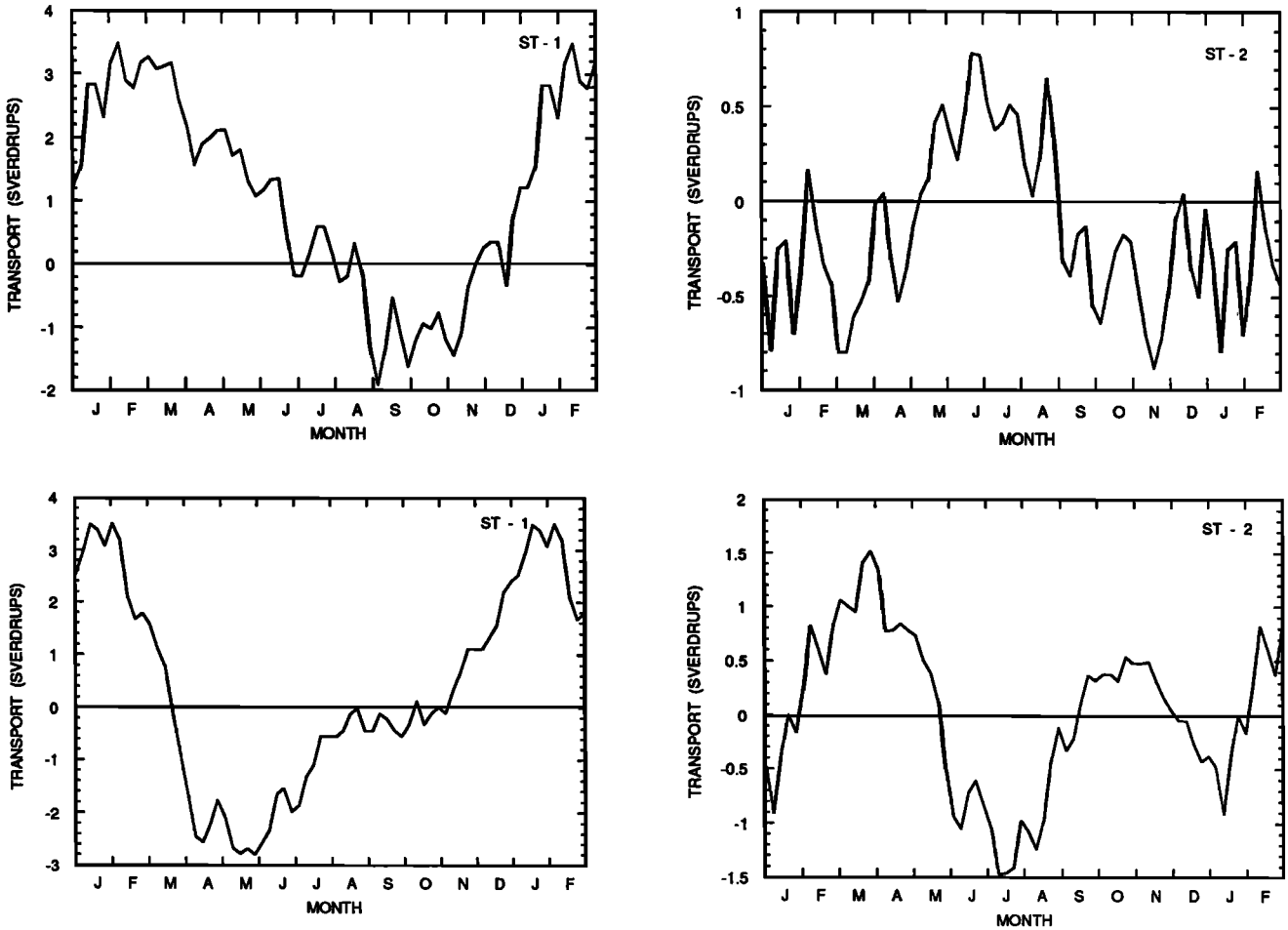

Fig. 5. Time series of mass transport. Transport (in sverdrups) is calculated using the model velocity and height data. Flows through ST-1 and ST-2 (see Figure 4) are displayed as functions of days. Positive transport indicates northward flow, while negative transport shows southward flow. Transport for the surface layer is above with the second layer below. Maximum transports in the upper layer, about 3.5 Sv, are seen in the western boundary current during February.

until July. Plates 1*e*, 1*f*, and 1*a* show that from July until spring (March), flow enters the basin from the north, circulates clockwise, and exits in the south.

The results in the lower layer are somewhat different. Flow changes direction three times during the year instead of once. In January, February, and March (Plates 2*a* and 2*b*) flow is cyclonic. This switches in spring and early summer (April–July). August, September, and October show flow returning to a cyclonic orientation. Finally, in November and December (Plate 2*f*) flow is anticyclonic.

More interesting is the height field in this area. In February a region of upwelling enters the Andaman Sea from the south. The upper layer thickness is 180 m along the southeast coast of the basin. The anticyclonic circulation surrounds a high value of upper layer thickness, 195 m. By March the upwelling region has propagated along the basin coastline and extends well into the Bay of Bengal. The upwelling pulse is followed in May by an area of downwelling. The center of the circulation, now cyclonic, is 180 m deep in the upper layer, and the downwelling signal along the coast reaches 195 m.

By June the upper layer is 215 m deep on the eastern side of the sea, stretching northward along the coast. Finally, in August, the center of the Andaman Sea is marked by a relatively deep upper layer (i.e., deep thermocline), 210 m, and flow is anticyclonic around it.

In the lower layer, flow in February is anticyclonic around a relatively thin region, 436 m. The southeast corner of the basin shows a thickening of the top two layers to about 450 m. By May this thick region has propagated around the whole sea, increasing to 460 m. In May the maximum thickness is in the center of the basin, and flow is anticyclonic around it. A region of upwelling then follows in June, propagates up the coast, and moves to the center of the basin by fall.

The calculations of mass transport in this area, made at locations ST-3, ST-4, and ST-5 (see Figure 4) are shown in Figure 6. Maximum transport along the east side of the sea, in the upper layer, is 2 Sv northward in mid-May and 1.5 Sv southward in early August. Transports in the lower layer reach 2 Sv in May, but the flow is southward, and in February the flow is northward.

Flow through the Great Channel (southern entry of the Andaman Sea), the area of largest transport, peaks in May as well, reaching 3.5 Sv northward in the upper layer. Flow exiting the sea in the upper layer becomes 5 Sv in early August. The lower layer experiences northward transport though ST-5 in late February and early March (about 4.2 Sv).

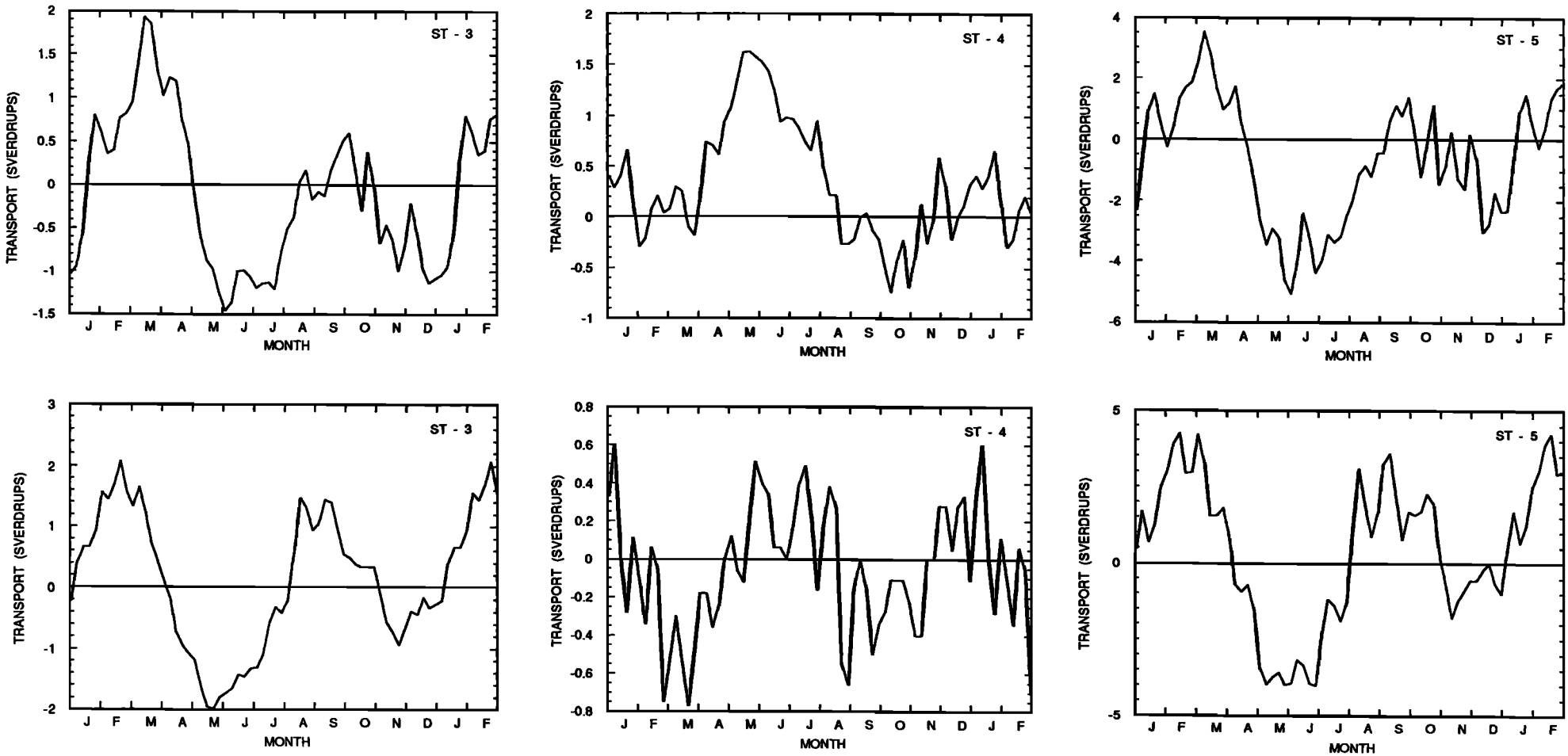

Fig. 6. Mass transport in the Andaman Sea. Transport (in sverdrups) is calculated using the model velocity and height data. Flows through ST-3, ST-4, and ST-5 (see Figure 4) are displayed as functions of days. Positive transport indicates northward flow through ST-3 and ST-5 and eastward flow into the basin through ST-4. Results for the upper layer are above and the lower layer below. A semiannual signal is seen in both layers. The two layers are not in phase, however. Maximum transport is seen in the upper layer during May and August and in the lower layer during February and May.

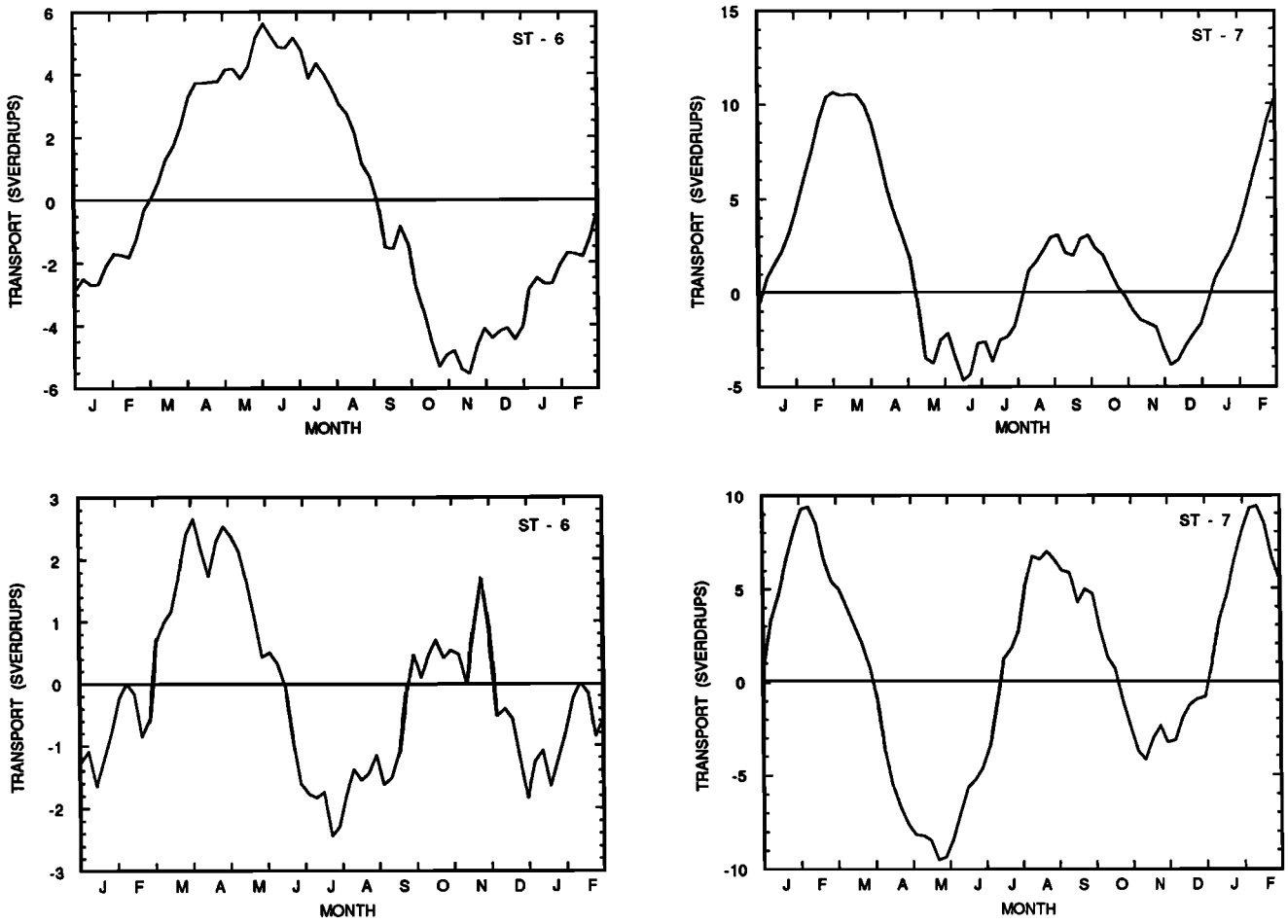

Fig. 7. Mass transport in the equatorial region. Transport in sverdrups is calculated using the model velocity and height data. Flows through ST-6, ST-7, ST-8, and ST-9 (see Figure 4) are displayed as functions of days. Positive transport indicates eastward flow through ST-6, ST-7, and ST-8 and northward flow into the basin through ST-9. A semiannual signal is seen in both the upper layer (top) and the lower layer (bottom). Similar to other areas, the two layers are not in phase. Maximum transport at the equator is seen in the upper layer during May and in the lower layer during February and May.

The maximum southward flow in this layer, 4 Sv, is during May and June.

4.3. *Equatorial Currents*

The final components of flow in this region are the currents in the equatorial region from 8°N down to 7°S. During the year, three distinct flows are generated in this area. In February the upper layer shows (Plate 1*a*) currents flowing toward the west between Sri Lanka (6°N) and 1°S. South of 1°S the flow is toward the east. The region centered at the equator, from 3°N to 3°S, is thinner (180 m) than the region just to the north and south (185 m). A region of downwelling (upper layer thickness of about 195 m) can be seen emerging from below Sumatra at 101°E.

In the next month, March, the thin region at the equator moves off the coast, toward the west, with counterclockwise flow around it. This results in westward flow north of 3°N and eastward flow from 3°N to the equator. South of the equator the flow is still to the east. The area of large upper layer thickness, which was off Sumatra in February, leaves the coast at the equator propagating westward. By May (Plate 1*c*), this signal has moved all the way across the region to 75°E. The upper layer thickness on the eastern side has increased to 200 m. The counterclockwise gyre north of the equator has moved to 78°E. Flow north of 4°N is weakly to the east while all other equatorial currents are to the west. In June the flow starts to follow the upper layer thickness contour, moving toward the east but splitting at about 80°E. Flow north of the equator is toward the east, while south of the equator it is more in a southeastward direction. Along the equator the flow is impeded by the thickening of the layer and turns south. The upper layer thickness reaches a maximum along the coast (210 m) this month; however, the region of downwelling is beginning to decrease. By August, as is shown in Plate 1*e* an area of upwelling occurs at 78°E. The downwelling pulse moves towards the coast at this time as well. Flow south of 4°S is to the west. North of 4°S, up to 3°N, the flow is to the east. North of 3°N, flow is again in the westward direction. Finally, in November, the equatorial flow to the east strengthens while the westward flow in the north weakens.

The second layer results show a relatively strong equatorial jet established in February. Flow within 2° of the equator is rapid, toward the east. Flow north and south of this region

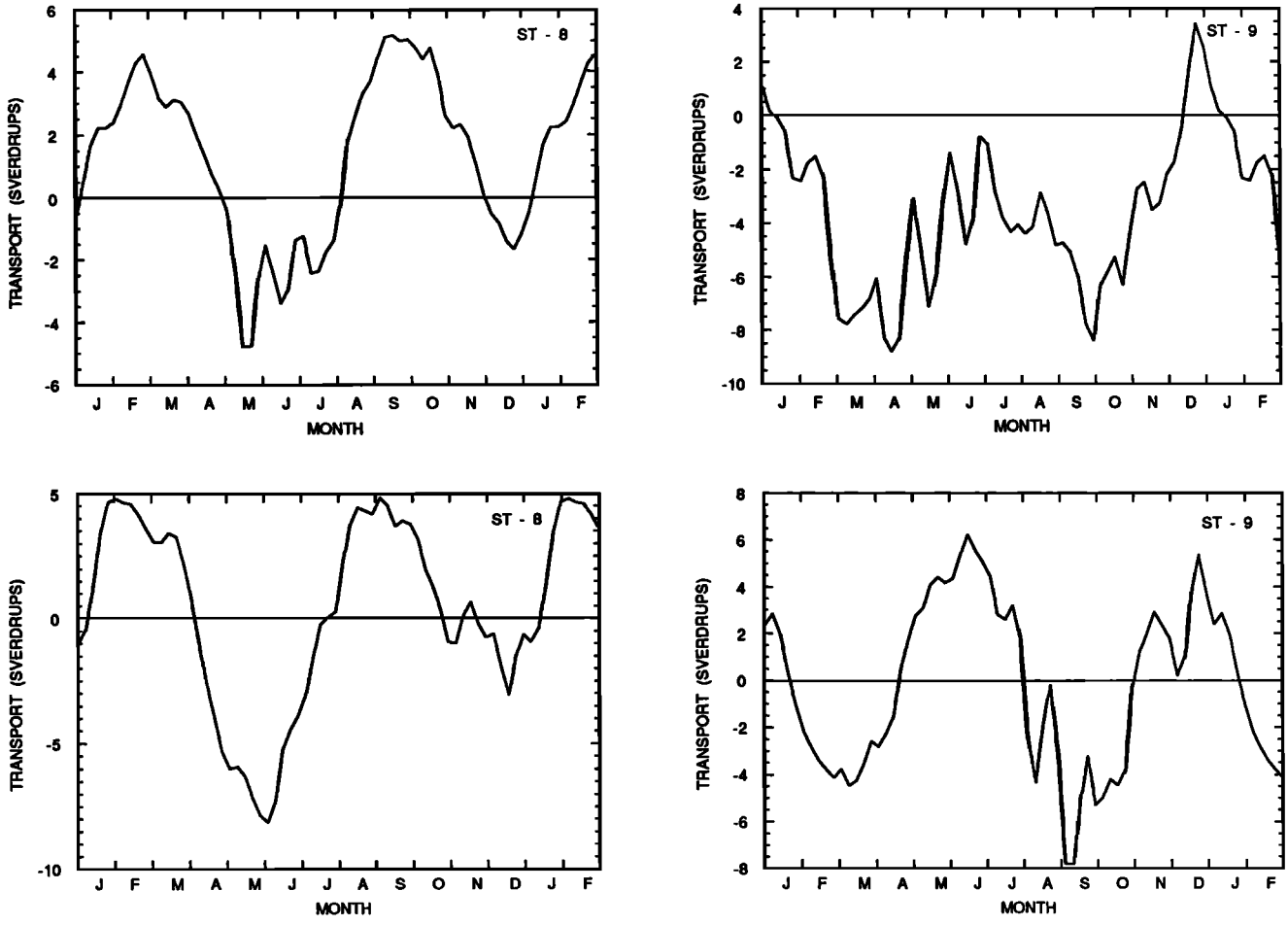

Fig. 7. (continued)

is weakly to the west. The region of high velocity is marked by a deep interface depth. In March the flow appears to reverse at about 85°E. Further east, two regions of deep layer thickness (457 m) develop, symmetric about the equator, with clockwise flow around the one north of the equator and counterclockwise flow around the southern one.

In May the two circulations have expanded across the region, producing strong westward flow at the equator and eastward flow north and south of the equator. This continues in June, with an upwelling signal, coming from the south, propagating to the north. At the equator the signal splits, with a large pulse traveling west and a smaller portion continuing north. Later in the summer, in August, two circulations develop around areas of low depth (440 m), counterclockwise in the north and clockwise in the south. There is strong eastward flow at the equator where the two systems meet. At the end of the year, in November, the flow is relatively weak, and at the equator it is toward the west.

The calculations of transport in the equatorial region, shown in Figure 7, show semiannual periods at all stations except in the upper layer above 3°N which is annual. It also becomes apparent that flow is out of phase in the two layers, as is sometimes seen in the other regions. From 3°N to 6°N (ST-6) the flow is baroclinic during most of the year. In the upper layer the transport is toward the east from May through October. It reaches a maximum of 5.5 Sv in August. During the rest of the year, November through April, it is to the west, with a maximum of 5.5 Sv in January. The lower layer, however, has net transport eastward during March, April, and May and again in October and November. The maximum during this time is 2.5 Sv during April. During the remainder of the year, transport is to the west. The maximum is 2.5 Sv during July.

The area further south, between 3°N and the equator (ST-7), shows greater transport. In the upper layer, from March through June and October through December, the transport is to the east. Throughout the month of May it exceeds 10 Sv. The maximum westward flow, 4.5 Sv, appears in August. At the same location in the second layer, eastward flow is found during January, February, and March and again in August, September, and October. The largest eastward transport is in February, 9.5 Sv, and the largest westward transport, again 9.5 Sv, is in May.

Finally, south of the equator, to 3°S (ST-8), transport in the upper layer is shown to be westward during July, August, and September, and again in February, in the upper layer. In the lower layer, flow is to the west in April, May, June, and July, and again in November, December, and January. Maximum transport in the upper layer is 5 Sv to the east in November and 5 Sv to the west in late July. The second layer has somewhat greater transport, with 8 Sv westward in early June and 5 Sv in late August and again in early February.

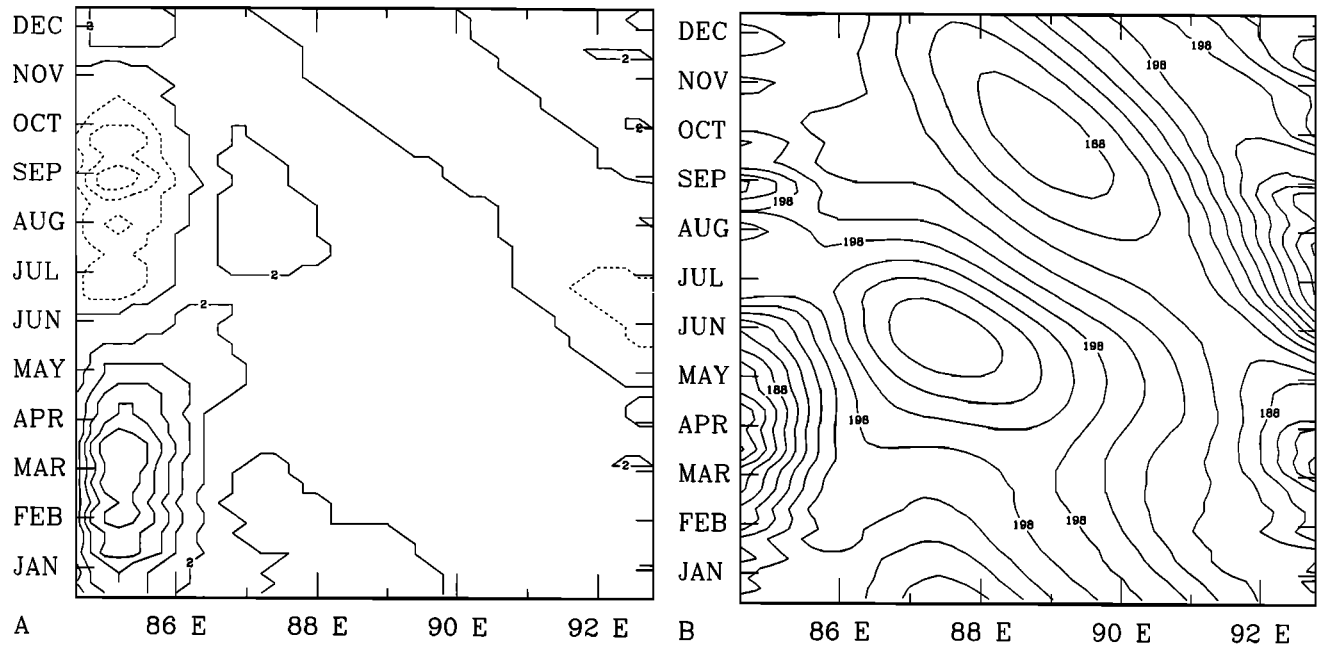

Fig. 8. (*a*) Zonal velocity in the upper layer at 18°N. The contour values are from −0.080 m s^{-1} (westward; dashed contour lines) to 0.120 m s^{-1} (eastward; solid contour lines) at an interval of 0.020 m s^{-1}. The annual change in direction of the western intensified current can be seen between 85°E and 86°E. The sloping contours indicate a wave traveling with western phase speed, calculated to be 0.035 m s^{-1}, with a period of 232 days. This is interpreted as a Rossby wave generated by a Kelvin wave that is traveling along the coast in the Bay of Bengal. (*b*) Upper layer thickness at 18°N. The contour values are from 178 m to 208 m at an interval of 2 m. Westward propagating Rossby waves are seen in the summer (upwelling) and again in fall (downwelling). A coastal Kelvin wave is also propagating along the east coast.

5. Temporal Variations

The time-varying signals of the model can be explored by means of various techniques. Many elements of the Indian monsoon system are periodic, ranging from the diurnal signal in rainfall to the annual shift in the winds [*Krishnamurti and Bhalme*, 1976]. These oscillations in the atmospheric conditions create oscillations in the oceanic system. It is also true that oscillations in the ocean can bring about fluctuations in the atmosphere, although atmospheric conditions are not incorporated in the model.

The most obvious signal associated with the monsoon region is the annual reversal in currents associated with the changing monsoon winds. As was previously discussed, currents in the Bay of Bengal, the Andaman Sea, and the equatorial region change direction at least once, sometimes twice, during the year. Spectral analysis of the transport data shows that in addition to these annual and semiannual signals there are other major frequencies inherent to the major current systems as reproduced by the model. Two significant peaks in the spectra of the transport time series appear in the 20- to 30-day range and in the 50- to 60-day range. The northern currents in the upper layer, including the eastern and western coasts of the Bay of Bengal, flow in the Andaman Sea, and the North Equatorial Current, all show peaks around 23 days. This same peak is seen at all stations (Figure 4) in the lower layer.

The equatorial currents show a peak at a 30-day period in the upper layer and a 26-day peak in the lower layer. Another strong signal is evident at a 60-day period in the equatorial region of both layers. This peak is found in the northern points at a somewhat shorter period of 50 days.

It has been suggested that oscillations at these frequencies observed in the tropical Indian Ocean are forced by atmospheric oscillations of similar frequency [*Madden and Julian*, 1972]. The model, however, reproduces these oscillations despite being forced by monthly mean winds. The fundamental period resolved in the wind forcing, therefore, is 60 days.

Effects on a seasonal scale also appear with the formation of waves at the equator and along the coast. An upwelling Kelvin wave, characterized by low upper layer thickness, appears in the model during early winter (Plate 1*a*). Traveling east along the equator, it hits the coast and reflects back as a downwelling, westward propagating Rossby wave. The maximum amplitude of this wave is seen leaving the coast of Sumatra in early summer (Plate 1*d*). Some of the energy of the Kelvin wave moves along the coast as two coastal Kelvin waves, one northward and the other southward. This signal can be found propagating the entire coastline around both the Andaman Sea and the Bay of Bengal.

A time-longitude plot shows that as these Kelvin waves travel along the coast, they excite Rossby waves which travel across the basin. In Figure 8*a*, zonal velocity is plotted since the configuration of the coast at 18°N is mainly in the east-west direction. One significant feature of this picture is the northwest/southeast sloping contour lines in the center of the region, 87°E to 93°E. The tilt indicates a westward propagating feature. Calculation of the slope of this line, in meters per second, yields the phase velocity of the westward signal at 0.035 m s^{-1}. *Gill* [1982] calculates that Rossby waves at 18°N will propagate west with a phase velocity of 0.047 m s^{-1}. This suggests that the signal appearing in the center of this plot is a Rossby wave that has been generated on the east coast of the bay.

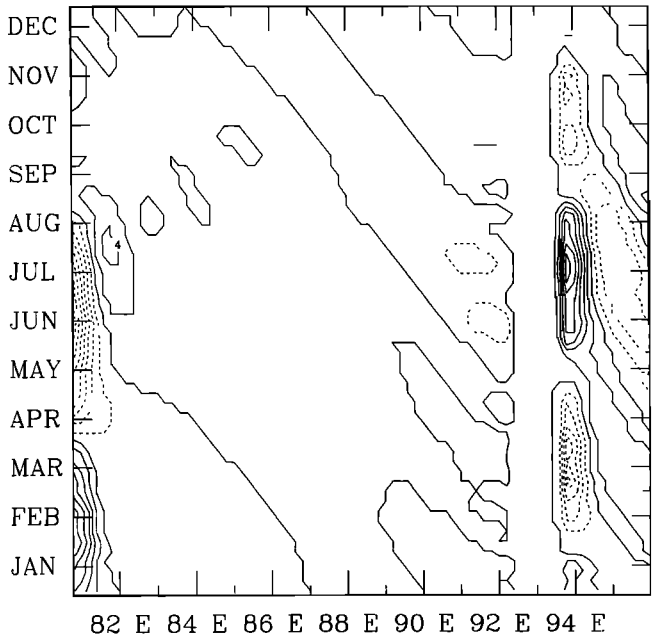

Fig. 9. Meridional velocity in the lower layer at 13°N. The contours are from -0.160 m s^{-1} (southward) to 0.160 m s^{-1} (northward) at an interval of 0.020 m s^{-1} (dashed contours represent southward velocity). The Andaman Islands block the signal between 92°E and 94°E. A westward propagating Rossby wave, generated by a coastal Kelvin wave, appears with phase speed of 0.047 m s^{-1} and period of 200 days as is evident in the sloping contours. The western intensification appears to change direction three times during the year (late May, mid-August, and late November).

The signal is lost on the western side of the bay as it interacts with the western boundary current. This western intensification appears in the contour plot between 85°E and 86°E. In the first half of the year, January to June, the flow is in the eastward direction. In February and March it reaches a maximum of 0.120 m s^{-1}. In June the flow switches direction and remains westward until December. The current is slightly weaker at this time of the year, with maximum velocity 0.080 m s^{-1} (westward).

A plot of the upper layer height field, Figure 8*b*, shows similar features. The westward sloping lines are again evidence of the Rossby wave generated in the east coast. The peaks in the contours in the eastern side of the bay show the coastal Kelvin waves which excite the Rossby waves. These Kelvin waves bring upwelling from January until May followed by downwelling in June through October. The peaks of the excited Rossby waves can be seen in this figure as they propagate westward.

Repeating this procedure for the second layer, at a lower latitude, reveals a similar result (Figure 9). The coastline at this latitude is more north-south; therefore meridional velocity is used (the intrusion of the Andaman Islands accounts for the gap in the contours in Figure 9 at 93°E). Maximum velocity, again found in the western boundary current, is 0.160 m s^{-1}. During January, February, and March this current flows to the north, in the lower layer, while in April through August it is southward. The westward propagating Rossby waves are evident. The phase is computed, from the slope of the lines, to be 0.050 m s^{-1}. The theoretical value [from *Gill*, 1982], is computed to be 0.054 m s^{-1}. The phase speed is higher at this latitude than the previous case (phase speed increases with decreasing latitude).

The results in the Andaman Sea (east of 92°E) show the current on the eastern side to be southward in February, March, and April and again in September, October, and November. During the rest of the year it is to the north.

More oscillations are seen in the equatorial waveguide. This is a region a few degrees wide, depending on the trapping scale of a particular wave, centered at the equator.

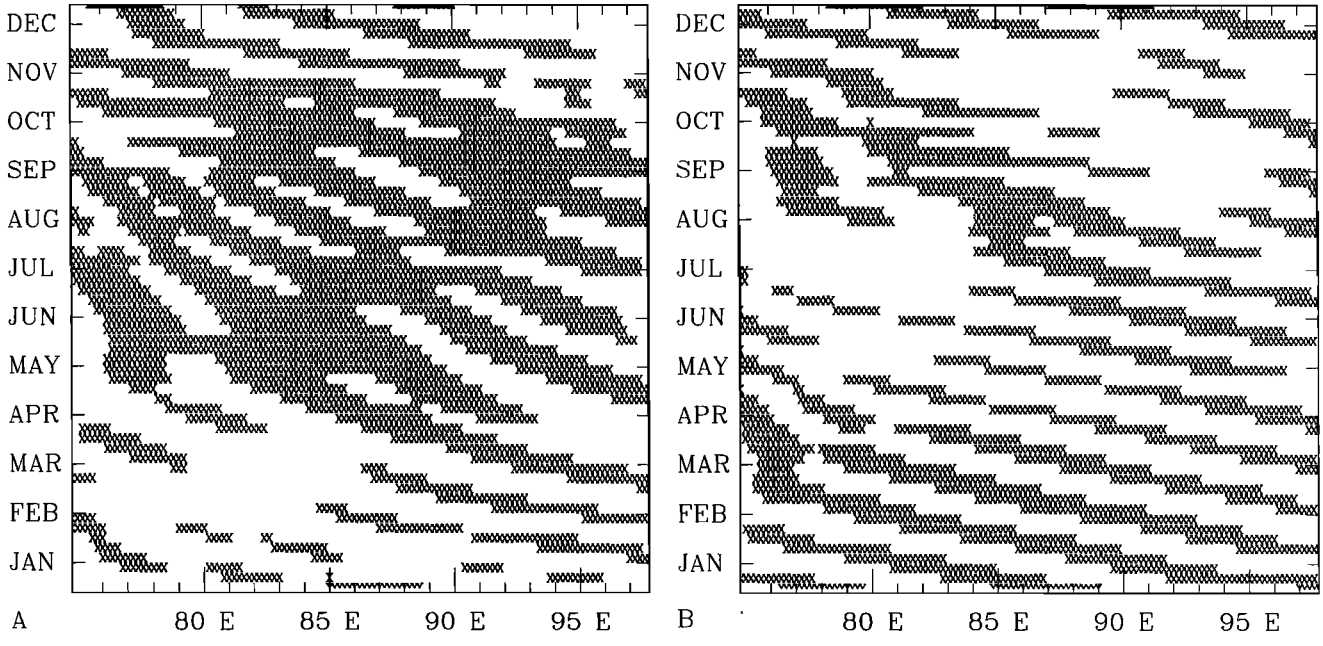

Fig. 10. Meridional velocity at the equator for (*a*) model upper layer, and (*b*) model lower layer. Velocities are from -0.080 m s^{-1} (southward) to 0.080 m s^{-1} (northward). In this representation, areas of southward velocity are shaded. The slope to these areas shows features with westward propagation, a phase speed of 0.300 m s^{-1}, and a period of about 30 days, interpreted as Yanai waves.

Waves generated in this region become trapped owing to the effects of the Coriolis force. Three of the lower-frequency waves (periods greater than 2 weeks) that propagate in this region are the eastward traveling Kelvin waves, the westward Rossby waves, and westward propagating mixed Rossby-gravity waves (Yanai waves). Plate 3 displays contours, plotted using a color scale, of the antisymmetric component of the upper layer height field along 3°N. The antisymmetric component is computed by subtracting the signal at 3°S from the signal at 3°N. Signals symmetric about the equator are therefore eliminated. The antisymmetric waves include even mode Rossby waves, which have relatively low frequencies, and the higher-frequency Yanai waves. Twice the time between minimum and maximum layer thickness indicates the wave period (found in Plate 3 to be 240 days). This, along with a computed phase velocity of 0.190 m s^{-1}, is indicative of a Rossby wave.

At the equator, the higher-frequency Yanai waves are seen. Both Figure 10*a* and 10*b* (upper and lower model layers, respectively) show a westward propagating feature with phase speed of 0.300 m s^{-1} and period of about 30 days. Using these values in the linear dispersion relationship for equatorial waves, these can be identified as Yanai waves. These waves have been observed in all oceans, and they were first seen in the Indian Ocean by *Luyten and Roemmich* [1982]. *Kindle and Thompson* [1989] studied Yanai waves in detail using a one and one-half layer model of the Indian Ocean.

6. Conclusions

The purpose of this study is to study the seasonal circulation in the Bay of Bengal. Because of the scarcity of measured data in this region, a three and one-half layer model, driven by climatological monthly mean winds, is used to examine the dynamics of this region of the Indian Ocean. This model accurately simulates the currents with slight deviations from available observations.

Flow in the Bay of Bengal is observed in the model results to be strongly anticyclonic, in the surface layer, in the winter months of December, January, February, and March. In spring and early summer, two circular flows develop, anticyclonic on the western side of the bay and cyclonic on the eastern side. In July and August the cyclonic circulation extends over the entire basin. Flow at this time is very weak, however. In the fall the two-gyre system forms again with the appearance of an anticyclonic circulation in the eastern half of the bay. By winter this flow has moved across the bay, and the process repeats itself. The second layer of the model shows a similar pattern, but it occurs slightly out of phase with the surface layer. This circulation pattern is in general agreement with observations. Some assumptions are made because the scale of the model is more detailed than the measured data.

Oscillations in these currents are illustrated through spectral analysis of transport data in this region. Significant peaks at 20- and 50-day periods are found at both the eastern and western sides of the bay. In addition, the results of the model height field show a coastal Kelvin wave, which originates at the equator, propagating around the entire western perimeter of the region (around both the Andaman Sea and the Bay of Bengal). This wave, when in the bay, excites westward propagating Rossby waves.

Flow in the Andaman Sea is observed to clockwise in the upper layer during most of the year. In spring and early summer it is counterclockwise. In contrast, flow in the lower layer reverses four times during the year. Measured data in this region is not very abundant, but the atlases that do exist show weak drift currents in the north-south direction fed by the equatorial currents. The model treats this region as more of an enclosed area, so a circular flow can develop. Significant oscillations occur in this region at periods of 25 and 50 days in the surface layer and 20 and 36 days in the lower layer.

Finally, currents in the equatorial region are examined. The NEC, SEC, and ECC are all represented by the model. Also, an equatorial jet appears in the monsoon transition periods, consistent with observations. Spectral analysis shows significant peaks at 30- and 60-day periods for currents in this region. Rossby and Yanai waves are also observed propagating westward in the equatorial wave guide.

Acknowledgments. This work was supported by a NASA Traineeship in Physical Oceanography funded by Oceanic Processes, NASA, by the Physical Oceanography Section of the Office of Naval Research and by NSF grant OCE-8811316 from the Physical Oceanography Section and the Climate Dynamics Section of NSF. Partial support was provided by the Florida State University through time granted on its Cyber 205 and Cray Y-MP supercomputers. The authors express their appreciation to Alan C. Davis for his assistance with computer computations and to Tommy Jensen for the use of his model computations.

References

Cane, M. A., On the dynamics of equatorial currents, With application to the Indian Ocean, *Deep Sea Res., Part A, 27*, 525–544, 1980.

Cutler, A. N., and J. C. Swallow, Surface currents of the Indian Ocean (to 25°S, 100°E): Compiled from historical data archived by the Meteorological Office, Bracknell, UK, *Rep. 187*, 8 pp., 37 charts, Inst. of Oceanogr., Wormley, England, 1984.

Deutsches Hydrographisches Institut, Monatskarten für den Indischen Ozean, *Publ. 2422*, Hamburg, Germany, 1960.

Düing, W., *The Monsoon Regime of the Currents in the Indian Ocean*, 68 pp., East-West Center Press, Honolulu, 1970.

Fein, J. S., and P. L. Stephens (eds.), *Monsoons*, 632 pp., John Wiley, New York, 1987.

Gent, P. R., K. O'Neill, and M. A. Cane, On the dynamical formulation of the large-scale momentum exchange between atmosphere and ocean, *J. Mar. Res., 24*, 105–112, 1983.

Gill, A. E., *Atmosphere-Ocean Dynamics*, 662 pp., Academic, San Diego, Calif., 1982.

Hastenrath, S., *Climate and Circulation of the Tropics*, 455 pp., Kluwer Academic, Hingham, Mass., 1985.

Hastenrath, S., and P. J. Lamb, *Climate Atlas of the Indian Ocean*, vol. 1, *Surface Climate and Atmospheric Circulation*, 19 pp., 97 charts, University of Wisconsin Press, Madison, 1979.

Hellerman, S., and M. Rosenstein, Normal monthly wind stress over the world ocean with error estimates, *J. Phys. Oceanogr., 13*, 1093–1104, 1983.

Jensen, R. G., A numerical study of the seasonal variability of the Somali Current, Ph.D. dissertation, 118 pp., Florida State Univ., Tallahassee, Feb., 1990.

Johns, B., A. D. Rao, S. K. Dube, and P. C. Sinha, Numerical modelling of tide surge interaction in the Bay of Bengal, *Philos. Trans. R. Soc. London, 313*, 507–535, 1985.

Kindle, J. C., and D. J. Thompson, The 26- and 50-day oscillations in the western Indian Ocean: Model results, *J. Geophys. Res., 94*, 4721–4736, 1989.

Krishnamurti, T. N., and H. N. Bhalme, Oscillations of a monsoon system, I, Observational aspects, *J. Atmos. Sci., 33*, 1937–1954, 1976.

Legeckis, R., Satellite Observations of a western boundary current in the Bay of Bengal, *J. Geophys. Res., 92*, 12,974–12,978, 1987.

Luther, M. E., Indian Ocean modeling, in *Further Progress in Equatorial Oceanography*, edited by E. Katz and J. Witte, pp. 303–316, Nova University Press, Dania, Fla., 1987.

Luther, M. E., and J. J. O'Brien, A model of the seasonal circulation in the Arabian Sea forced by observed winds, *Prog. Oceanogr.*, *14*, 353–385, 1985.

Luther, M. E., J. J. O'Brien, and A. H. Meng, Morphology of the Somali Current system during the southwest monsoon, in *Coupled Ocean-Atmosphere Models*, edited by J. C. J. Nihoul, pp. 405–437, Elsevier Science, New York, 1985.

Luyten, J. R., and D. H. Roemmich, Equatorial currents at semiannual period in the Indian Ocean, *J. Phys. Oceanogr.*, *12*, 406–413, 1982.

Madden, R. A., and P. R. Julian, Description of global-scale circulation cells in the tropics with a 40–50 day period, *J. Atmos. Sci.*, *29*, 1109–1123, 1972.

McClain, E. P., W. G. Pichel, and C. C. Walton, Comparative performance of AVHHR-based multichannel sea surface temperatures, *J. Geophys. Res.*, *90*, 11,587–11,601, 1985.

Molinari, R. L., D. Olson, and G. Reverdin, Surface current distributions in the tropical Indian Ocean derived from compilations of surface buoy trajectories, *J. Geophys. Res.*, *95*, 7217–7238, 1990.

O'Brien, J. J., The diffusive problem, in *Advanced Physical Oceanographic Numerical Modelling*, edited by J. J. O'Brien, pp. 127–144, D. Reidel, Norwell, Mass., 1986.

O'Brien, James J., and H. E. Hurlburt, Equatorial jet in the Indian Ocean: Theory, *Science*, *184*, 1075–1077, 1974.

Piccard, G. L., and W. J. Emery, *Descriptive Physical Oceanography*, 249 pp., Pergamon, New York, 1982.

Rao, R. R., R. L. Molinari, and J. F. Festa, Evolution of the climatological near-surfacer thermal structure of the tropical Indian Ocean, *J. Geophys. Res.*, *94*, 10,801–10,815, 1989.

Somayajulu, Y. K., T. V. R. Murty, S. P. Kumar, and J. S. Sastry, Hydrographic characteristics of central Bay of Bengal waters during southwest monsoon of 1983, *Indian J. Mar. Sci.*, *16*, 207–217, 1987.

Subbaramayya, I., and S. R. Rao, Secular variations of sea surface temperature in the Bay of Bengal, *Mahasagar*, *19*, 165–173, 1986.

Tchernia, P., *Descriptive Regional Oceanography*, 253 pp., Pergamon, Elmsford, N. Y., 1980.

Woodberry, K. E., M. E. Luther, and J. J. O'Brien, The wind-driven seasonal circulation in the southern tropical Indian Ocean, *J. Geophys. Res.*, *94*, 17,985–18,002, 1989.

Wyrtki, K., Physical oceanography of the Southeast Asian waters, Scientific results of the maritime investigations of the South China Sea and Gulf of Thailand 1959–1961, *NAGA Rep. 2*, 195 pp., Scripps Inst. of Oceanogr., La Jolla, Calif., 1961.

Wyrtki, K., *Oceanographic Atlas of the International Indian Ocean Expedition*, 531 pp., National Science Foundation, Washington, D. C., 1971.

Wyrtki, K., An equatorial jet in the Indian Ocean, *Science*, *181*, 262–264, 1973.

M. E. Luther, Department of Marine Science, University of South Florida, 140 Seventh Avenue South, St. Petersburg, FL 33701.

J. J. O'Brien, Mesoscale Air-Sea Interaction Group, Mail Stop B-174, Love 012, Florida State University, Tallahassee, FL 32306.

J. T. Potemra, STX, NASA Goddard Space Flight Center, Code 971, Greenbelt Road, Greenbelt, MD 20771.

(Received September 17, 1990;
revised March 13, 1991;
accepted March 18, 1991.)